American Mineralogist, Volume 93, pages 53–62, 2008

Pressure-induced structural deformation and elastic behavior of wairakite

SILVIA ORI,[1] SIMONA QUARTIERI,[2,*] GIOVANNA VEZZALINI,[1] AND VLADIMIR DMITRIEV[3]

[1]Dipartimento di Scienze della Terra, Università di Modena e Reggio Emilia, via S. Eufemia 19, 41100 Modena, Italy
[2]Dipartimento di Scienze della Terra, Università di Messina, Salita Sperone 31, 98166 Messina S. Agata, Italy
[3]Swiss-Norwegian Beam Lines at ESRF, BP220, 38043 Grenoble Cedex, France

ABSTRACT

The elastic behavior and the high-pressure structural evolution of the zeolite wairakite [ideal chemical formula $Ca(Al_2Si_4O_{12})\cdot 2H_2O$, space group *I2/a*], the Ca-analog of analcime, have been investigated by means of in-situ synchrotron X-ray powder diffraction from ambient pressure to 7.8 GPa, and upon decompression. No complete X-ray amorphization is observed up to the highest investigated pressure, and the original unit-cell parameters are recovered upon decompression. The Rietveld structural refinements of the powder patterns converged successfully up to 2.5 GPa; above this pressure, a phase transition to triclinic symmetry is observed and only the unit-cell parameters were refined. An overall reduction of about 14% of the unit-cell volume between 0.0001 and 7.0 GPa is observed, demonstrating that wairakite is much more flexible upon compression than upon heating. The pressure dependence of the cell parameters is strongly anisotropic and larger after the transition to the triclinic space group. The elastic parameters refined with a second-order Birch-Murnaghan Equation of State are $V_0 = 2536(4)$ Å^3, $K_0 = 39(3)$ GPa, and $V_0 = 2632(38)$ Å^3, $K_0 = 24(3)$ GPa, for the monoclinic and triclinic phases, respectively.

The structure distortion of monoclinic wairakite, proceeding via tetrahedral tilting, induces deformations in the 4-, 6-, and 8-membered rings and an increase in the extra-framework Ca coordination number. A comparative discussion of the compressibility behavior of wairakite and analcime is reported.

Keywords: HP studies, XRD data, crystal structure, wairakite, phase transition, compressibility measurements

INTRODUCTION

Wairakite [ideal formula $Ca(Al_2Si_4O_{12})\cdot 2H_2O$] is an uncommon zeolite first found by Steiner (1955) at Wairakei (New Zealand) and described as the Ca-analog of analcime. It occurs widely in low-grade metamorphic rocks, sedimentary environments, and hydrothermal areas (Gottardi and Galli 1985; Tschernich 1992; Bish and Ming 2001). Wairakite forms a continuous solid solution series with analcime [$Na_2(Al_2Si_4O_{12})\cdot 2H_2O$], and this name applies to the zeolites with ANA structural type (Baerlocher et al. 2001) with Ca as the most abundant extra-framework cation (Coombs et al. 1997). The same topology ANA is also shared by leucite, pollucite, hsianghualite, and several synthetic phases (Baerlocher et al. 2001).

The structurally related zeolite analcime has been described in a variety of different symmetries from cubic to triclinic. Several authors (Mazzi and Galli 1978; Hazen and Finger 1979) suggested that the reason for such of wide range of symmetries could be a different Si/Al distribution. Concerning wairakite, its crystal structure was determined by Takeuchi et al. (1979) on a monoclinic sample from Onikobe (Japan) in the space group *I2/a*. Henderson et al. (1998) determined the structure of the synthetic counterpart by means of Rietveld analysis.

The thermal stability and high-temperature (HT) behavior of wairakite was studied by Seryotkin et al. (2003) by means of single-crystal X-ray diffraction and detailed structural information is available in the range between 20 and 600 °C. The main feature is the reversible phase transformation, at about 150 °C, from monoclinic *I2/a* to tetragonal $I4_1/acd$, with no fundamental change of the framework.

The only previous study of the high-pressure (HP) stability of wairakite was performed by Goryainov et al. (1999) with Raman spectroscopy on a single crystal mounted in a diamond anvil cell, using both water and glycerol as pressure transmitting media. These authors observed three phase transitions at 17.5, 31.3, and 67.0 kbar, interpreted as due to a decrease of the crystal symmetry along the sequence *I2/a*, $P2_1/a$, $P\bar{1}$, *P*1. In particular, significant variations in shape and position of the bands related to O-T-O vibrational modes were observed upon compression. Significant broadening of bands and nonreversal of the *P*-induced transitions were attributed to amorphization, which was complete at about 82 kbar. Some other HP data are reported by the same authors (Goryainov et al. 1996) for dehydrated wairakite studied with the same spectroscopic technique. In this case, an irreversible phase transition occurs at 34 kbar, attributed to polyhedral tilting. However, no details on any compressed crystal structure

* E-mail: simona.quartieri@unimore.it

are available.

The aim of this work is to investigate the elastic behavior and the HP-structural evolution of wairakite by means of in-situ synchrotron X-ray powder diffraction (XRPD). Our results will be compared with those obtained on analcime (Gatta et al. 2006) to single out the influence of the Si/Al ordering and the type of extra-framework cation on the compressibility and on the HP deformation mechanisms of these isotypic zeolites. Moreover, the structural behavior of wairakite under HP and HT will be compared.

Wairakite crystal structure

In the wairakite structure (Takeuchi et al. 1979), described by Gottardi and Galli (1985) as formed by singly connected 4-ring chains, two secondary building units are recognized: four- and six-membered rings of tetrahedra. The maximum symmetry of ANA topology is $Ia\bar{3}d$. Two channel systems are present: irregular channels formed by distorted eight-membered rings along [110], and regular channels formed by six-membered rings along the [111] direction. The framework symmetry is lowered to the space group $I2/a$ by the distribution of the extra-framework cations Ca and by the Al ordering on two preferred tetrahedra (T2A and T2B) (Takeuchi et al. 1979). The Al fractions of these two tetrahedra are identical. Among the extra-framework sites, two are fully occupied by water molecules and four by cations. Only one of these cation sites (M2) is almost completely occupied by Ca, while the others (M1, M12A, M12B) show a very low occupancy of Na. Wairakite and analcime present the same coordination geometry of the extra-framework cation polyhedra, which are regular octahedra formed by two water molecules at the apices and four framework O atoms belonging to the two tetrahedra mainly centered by Al.

Experimental methods

Wairakite used in this study comes from the type locality Wairakei (New Zealand) (Steiner 1955). The electron microprobe analysis was carried out at the Earth Science Department of University of Modena and Reggio Emilia, using an ARL-SEMQ instrument in wavelength dispersive mode, operating at 15 kV and with a beam current of 20 nA and diameter of 20 μm. The standards used were Amelia albite for Si, Al, and Na, AB microcline for K, paracelsian for Ba, and synthetic Di85-JD15, AN70 glass, Sr-anorthite, and P140 olivine for Mg, Ca, Sr, and Fe, respectively. The data acquisition and processing were performed using the PROBE program (Donovan 1995). The water content is from Steiner (1955). The corresponding formula is $(Ca_{7.12}Na_{1.21}K_{0.03}Sr_{0.02})$ $(Al_{15.74}Si_{32.31}O_{96})\cdot 16.43\ H_2O$. The unit-cell parameters determined at ambient conditions on the powder inside the DAC are a = 13.6921(5) Å, b = 13.6500(4) Å, c = 13.5672(3) Å, β = 90.508(3)°, and V = 2535.56 (8) Å^3.

Synchrotron X-ray powder diffraction experiments

The high-pressure XRPD experiments were performed at the SNBL1 (BM01a) beamline at European Synchrotron Radiation Facility (ESRF) with fixed wavelength of 0.7 Å, using a modified Merril-Bassett DAC (Miletich et al. 2000) and silicone oil as the non-penetrating P-transmitting medium. These conditions were chosen to allow the comparison of wairakite compressibility with those of the other zeolites studied by our group using the same non-penetrating P-transmitting medium (Vezzalini et al. 2001; Ballone et al. 2002; Ferro et al. 2002; Arletti et al. 2003; Fois et al. 2005a, 2005b; Betti et al. 2007). The pressure was measured using the ruby fluorescence method (Forman et al. 1972) on the non-linear hydrostatic pressure scale (Mao et al. 1986). The estimated error in the pressure values is 0.1 GPa. A MAR345 detector (pixel dimension 150 μm) was used at a fixed distance of 230 mm from the sample; the exposure time was 120 s for all pressure points. One-dimensional diffraction patterns were obtained in the 2θ range 0–47° by integrating the two dimensional images with the program FIT2D (Hammersley et al. 1996) and are reported in Figure 1.

The experiments were performed from ambient pressure (P_{amb}) up to 7.8 GPa, with ΔP increments of 0.2–0.6 GPa. Sample was equilibrated for about 30 min at each measured pressure. Three other patterns were collected while decompressing the sample up to P_{amb} [5.7 (rev), 3.4 (rev), P_{amb}(rev), in the following and in tables]. As a whole, 27 spectra were collected.

Lattice parameters and structural refinements strategy

Due to the low quality of the powder patterns collected in the highest-pressure regime, the data analysis was performed only up to 7.0 GPa. Two different strategies were adopted in the two ranges P_{amb}–2.5 and 3.2–7.0 GPa, whereas in the first P range complete Rietveld structural refinements were performed, above 2.5 GPa a P-induced symmetry lowering was observed and only the unit-cell values were extracted from the diffraction patterns.

The Rietveld profile fitting of eight patterns in the range P_{amb}–2.5 GPa and of one pattern collected at P_{amb} after pressure release were performed in the 2θ range 3–36.3° using of the GSAS package (Larson and Von Dreele 1996) with the EXPGUI (Toby 2001) interface. The atomic coordinates of the adopted structural model are from Takeuchi et al. (1979). The experimental intensities were corrected for the absorption of the Be backing plates. The background curves were fitted by a Chebyshev polynomial with an average of 10 coefficients in the 2θ range 4–10.7° and 20 coefficients for the range 10.7–36.3°. The pseudo-Voigt profile function proposed by Thomson et al. (1987) and cut-off of the peak intensity was applied.

Soft-constraints were applied to the T-O distances and gradually released after the initial stages of refinement. The isotropic displacement parameters were constrained in the following way: the same value was used for all tetrahedral cations (as suggested by the results of the single-crystal structure refinement of wairakite at ambient conditions by Takeuchi et al. 1979), a second one for all framework O atoms, a third for Ca extra-framework cations and a last one for water molecules. The displacement factor of Na cation was fixed in all refinements at the value of 0.04 Å^2 as reported in Takeuchi et al. (1979). In 2.1 and 2.5 GPa refinements, the

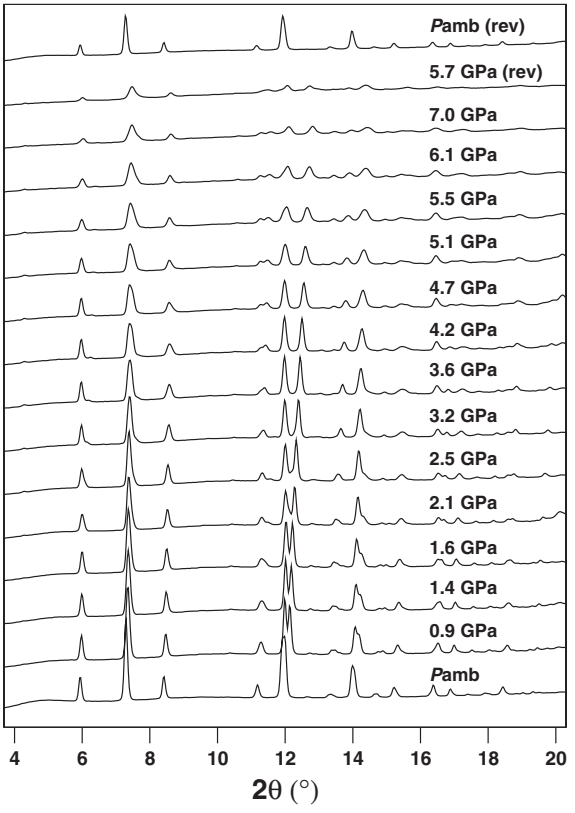

Figure 1. Selected integrated powder patterns of wairakite as a function of pressure, reported in the 2θ range 4–20°. The powder patterns at the top of the figure were collected during decompression.

displacement of water O atoms and Ca were fixed at the values obtained at 1.6 GPa; in the P_{amb}(rev) refinement the displacement parameters of water O atoms were fixed to the P_{amb} values. The water sites were assumed fully occupied in all the refinements. The unit-cell parameters of wairakite were allowed to vary for all refinement cycles. In the final cycles, only the fractional coordinates and the isotropic displacement factors of all the atoms were refined. Occupancy factors of extra-framework cations were refined at P_{amb} and fixed at the obtained values in the other refinements. Scattering factors (Cromer and Waber 1974) for neutral atoms were used for Si, Al, and framework O atoms; scattering factors for ionized atoms were used for Ca and water O atoms.

At P_{amb}, the whole structure of Takeuchi et al. (1979) was used as starting model and the same labeling is assumed. As the occupancies of the extra-framework sites M11 and M12A resulted in very low (or even negative) values and their positions were very unstable during the refinement cycles, these sites were then omitted. The occupancy of M2 site is very similar to that reported for single-crystal refinement (Takeuchi et al. 1979), while that of M12B is higher. In this way the resulting number of electrons obtained by the refinement of our sample, which is 142, is in perfect agreement with that obtained from its chemical analysis, which is 140.

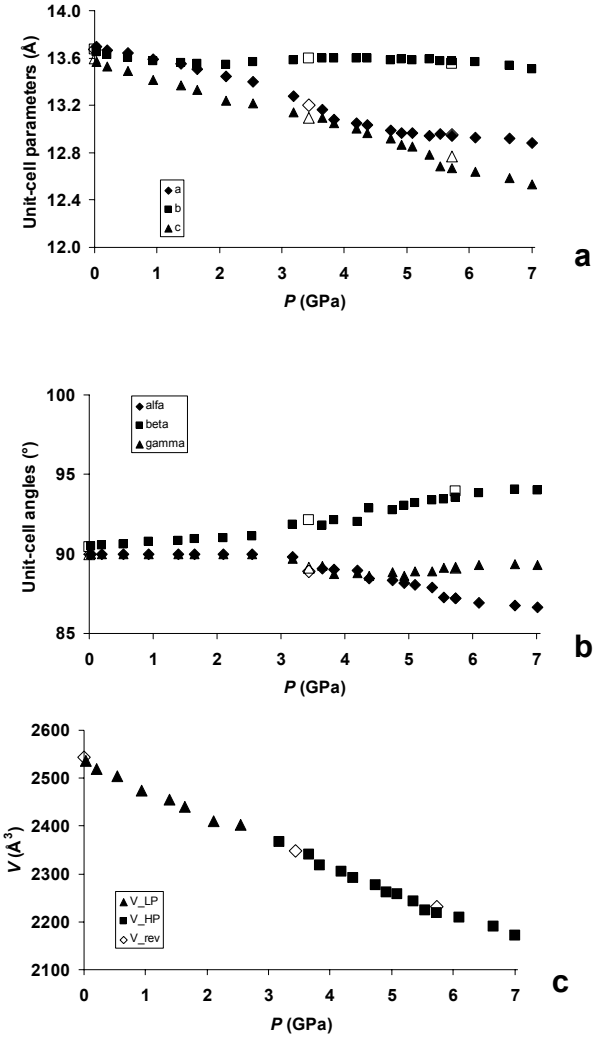

FIGURE 2. Variation of wairakite lattice parameters as a function of pressure. (**a**) unit-cell axes; (**b**) unit-cell angles; (**c**) unit-cell volume. The errors associated with the cell parameters are smaller than the symbols used. Open symbols are associated to the lattice values determined during decompression.

The Rietveld refinement of the powder patterns converged successfully up to 2.5 GPa, even if, at this last pressure, R_{F^2} value was higher than 20, suggesting an initial step of a phase transition. Above this pressure, the difficulty in the structural refinement reinforced the hypothesis of a phase transition. At 3.2 GPa, the unit-cell symmetry indicated by TREOR program (Werner et al. 1985)—used for indexing and space group determination—was $P\bar{1}$, consistent with that found by Goryainov et al. (1999) by HP-Raman spectroscopy at about 3 GPa, and at the *P*-induced phase transition in analcime (Gatta et al. 2006). Because of the consequent increase of the independent parameters and of the limited quality of the powder patterns, any attempt of structural refinements of the triclinic polymorph failed and only the unit-cell values were extracted from the diffraction data using the Le Bail whole pattern fitting by GSAS package (Le Bail et al. 1988; Larson and Von Dreele 1996). During these refinements the background was graphically fit, and not refined, to avoid divergence effects. The refined cell parameters as a function of pressure are reported in Table 1 and Figure 2.

The *P*-induced structural modifications of monoclinic wairakite were studied on the basis of nine structural refinements at P_{amb}, 0.2, 0.4, 0.9, 1.4, 1.6, 2.1, and 2.5 GPa and at ambient conditions after pressure release [P_{amb}(rev)]. Tables 2–5 report the refinement details and the structural data for the selected refinements at P_{amb}, 0.9, 2.1 GPa, and at P_{amb}(rev). Figures 3–6 show selected projections of monoclinic wairakite structure at the initial and final pressure values of the stability range of the (P_{amb} and 2.1 GPa) and after pressure release [P_{amb}(rev)].

RESULTS

Elastic behavior

Figure 1 reports selected experimental powder patterns of wairakite as a function of pressure. The peak intensities generally decrease and the peak profiles become broader with increasing pressure. These effects can be due to several factors, such as an increase in the long-range structural disorder, and the presence of microstrains caused by deviatoric stress in the *P*-transmitting medium (Yamanaka et al. 1997; Weidner et al. 1998; Fei and Wang 2000; Lee et al. 2002a, 2002b).

The HP XRPD data demonstrate that wairakite does not undergo complete amorphization up to the highest investigated pressure. Moreover, the ambient pressure pattern features, but not the peak intensities, are recovered upon decompression. These results are in partial disagreement with those of Goryainov et al. (1999), who describe as reversible only the phase transition at 17.5 kbar, but report a complete irreversibility for the *P*-induced amorphization occurring between about 7 and 8 GPa. These discrepancies could be ascribed to both the different investigation techniques used for the HP studies, and to the use of a single crystal instead of a powdered sample.

From the inspection of Figure 2 and Table 1, we can observe a reduction of about 5 and 9%, for the monoclinic and the triclinic unit-cell volume, respectively, and an overall reduction of about 14% of the unit-cell volume in the whole investigated *P* range. The unit-cell axes decreases in the whole pressure range are about 6, 1, and 8% for *a*, *b*, and *c*, respectively. Actually, the parameter *a* decreases only up to about 5 GPa, while it is roughly constant after this pressure and *b* is substantially independent from *P*. Concerning the unit-cell angles, β increases of about 4% over the complete *P* range, with a larger slope after the transition pressure; α and γ decrease of about 4 and 1% , respectively. Between 5 and 6 GPa, some cell parameters undergo a further slight slope change.

Based on the unit-cell parameter values measured after decompression, we observe that the monoclinic to triclinic phase transition is reversible, even if the unit-cell parameters of the ambient unit cell are not completely recovered. The *P*-*V* data

TABLE 1. Unit-cell parameters of both monoclinic and triclinic wairakite at the investigated pressures

P (GPa)	a (Å)	b (Å)	c (Å)	α (°)	β (°)	γ (°)	V (Å^3)
P_{amb}	13.6921(5)	13.6500(4)	13.5672(3)	–	90.508(3)	–	2535.56(8)
0.2	13.6688(4)	13.6262(4)	13.5250(3)	–	90.570(4)	–	2518.98(9)
0.5	13.6435(4)	13.6074(4)	13.4880(2)	–	90.626(3)	–	2503.94(7)
0.9	13.5875(7)	13.5728(6)	13.4140(3)	–	90.747(4)	–	2473.6(1)
1.4	13.5483(7)	13.5591(6)	13.3681(2)	–	90.849(4)	–	2455.50(8)
1.6	13.5092(7)	13.5544(6)	13.3273(3)	–	90.926(6)	–	2440.0(1)
2.1	13.441(2)	13.542(1)	13.241(1)	–	91.02(2)	–	2409.7(4)
2.5	13.451(3)	13.574(2)	13.216(1)	–	90.85(3)	–	2402.8(6)
3.2	13.278(1)	13.580(1)	13.137(1)	89.81(1)	91.85(1)	89.70(1)	2367.4(4)
3.6	13.164(2)	13.594(1)	13.092(1)	89.05(1)	91.82(1)	89.24(1)	2341.0(5)
3.8	13.078(2)	13.593(1)	13.049(2)	88.99(1)	92.14(1)	88.73(1)	2317.1(5)
4.2	13.050(1)	13.598(1)	13.000(2)	88.99(1)	92.01(1)	88.80(1)	2304.7(5)
4.4	13.031(1)	13.596(1)	12.964(1)	88.45(1)	92.87(1)	88.65(1)	2292.3(2)
4.7	12.991(2)	13.584(1)	12.920(1)	88.36(1)	92.73(1)	88.83(1)	2275.8(4)
4.9	12.969(2)	13.592(1)	12.865(1)	88.17(1)	93.01(1)	88.62(1)	2262.6(2)
5.1	12.964(1)	13.581(1)	12.853(1)	88.03(1)	93.19(1)	88.89(1)	2257.7(2)
5.4	12.942(1)	13.588(1)	12.786(1)	87.91(1)	93.39(1)	88.88(1)	2242.6(2)
5.5	12.955(1)	13.574(1)	12.687(1)	87.29(1)	93.46(1)	89.14(1)	2224.6(2)
5.7	12.942(1)	13.573(1)	12.673(2)	87.19(1)	93.56(1)	89.16(1)	2218.9(3)
6.1	12.926(1)	13.569(1)	12.639(2)	86.94(1)	93.86(1)	89.29(1)	2208.3(3)
6.6	12.918(2)	13.536(2)	12.584(2)	86.77(2)	94.08(1)	89.38(1)	2191.1(3)
7.0	12.879(3)	13.509(2)	12.534(2)	86.65(2)	93.98(1)	89.32(2)	2171.5(4)
5.7 (rev)	12.951(3)	13.549(3)	12.768(3)	87.23(2)	93.96(2)	89.15(2)	2232.0(10)
3.4 (rev)	13.204(3)	13.595(1)	13.095(3)	88.92(2)	92.11(1)	89.11(2)	2348.5(7)
P_{amb}(rev)	13.678(2)	13.674(2)	13.5977(6)	–	90.442(7)	–	2543.2(2)

Note: 5.7 (rev), 3.4 (rev), P_{amb}(rev) are three patterns collected while decompressing the sample up to P_{amb}.

TABLE 2. Details of structural refinements of monoclinic wairakite at selected pressures

	P_{amb}	0.9 GPa	2.1 GPa	P_{amb}(rev)
a (Å)	13.6921(5)	13.5875(7)	13.441(2)	13.678(2)
b (Å)	13.6500(4)	13.5728(6)	13.542(1)	13.674(2)
c (Å)	13.5672(3)	13.4140(3)	13.241(1)	13.5977(6)
α (°)	90.0	90.0	90.0	90.0
β (°)	90.508(3)	90.747(4)	91.02(2)	90.442(7)
γ (°)	90.0	90.0	90.0	90.0
Cell volume (Å^3)	2535.56(8)	2473.6(1)	2409.7(4)	2542.2(2)
R_p (%)	0.57	0.56	4.48	0.98
R_{wp} (%)	0.81	0.76	2.63	1.67
R_{F^2} (%)	5.77	7.18	18.50	10.28
χ^2	0.927	1.497	15.82	0.860
No. of variables	102	107	104	101
No. of observations	1146	1153	1142	1069
No. of reflections	964	950	965	963

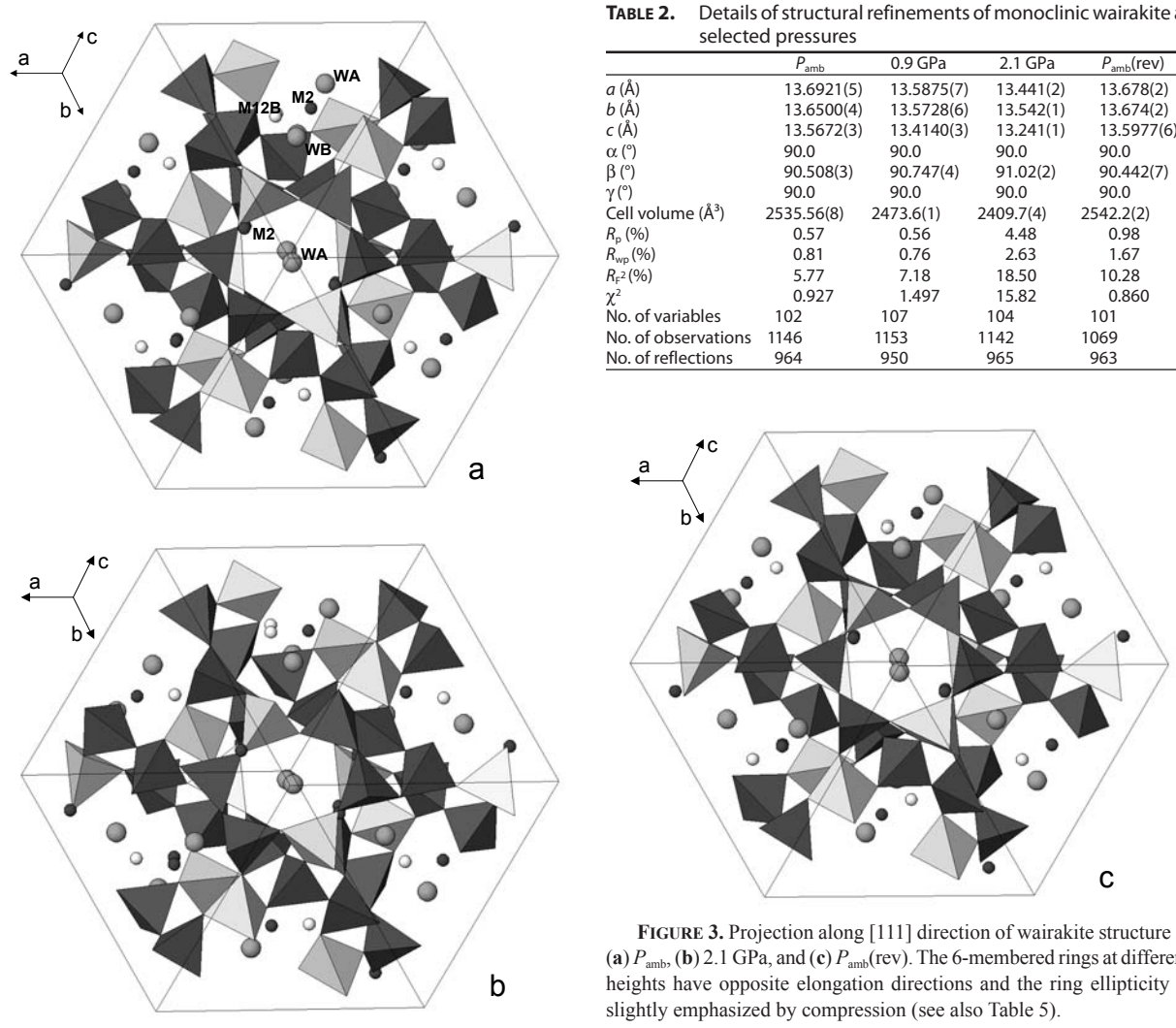

FIGURE 3. Projection along [111] direction of wairakite structure at (**a**) P_{amb}, (**b**) 2.1 GPa, and (**c**) P_{amb}(rev). The 6-membered rings at different heights have opposite elongation directions and the ring ellipticity is slightly emphasized by compression (see also Table 5).

of the monoclinic and triclinic polymorphs were fitted with a second-order Birch-Murnaghan Equation of State (II-BM-EoS, Birch 1947) using the EOS-Fit V5.2 program (Angel 2001). The elastic parameters were obtained, using the data weighted by the uncertainties in P and V: $V_0 = 2536(4)$ Å^3, $K_0 = 39(3)$ GPa and $V_0 = 2632(38)$ Å^3, $K_0 = 24(3)$ GPa, for the monoclinic and triclinic phases, respectively.

P-induced structural deformations in monoclinic wairakite

Framework. The atomic positions of the Si/Al-framework in wairakite, refined in this study, are in excellent agreement with those reported by Takeuchi et al. (1979) for the single-crystal study. Based on the similarity of the T-O bond distances, the same (Si,Al) distribution in the tetrahedra can be assumed.

The main deformation mechanism of the wairakite tetrahedral framework, consisting of tetrahedral tilting, is clearly visible in Figures 3–6 and is expressed in Table 5 by the ellipticity ratios ε. This parameter is defined as the half of the ratio between the sum of the two shortest diameters and the longest one for the 6-membered ring (6mR), and as the ratio between the shortest and the longest diameters for the 4-membered ring (4mR) (Gatta et al. 2006). The projection along [111] (Fig. 3) shows that the 6-membered rings at different heights (6mR-1 and 6mR-2) have opposite elongation directions and that the ring ellipticity of the 6mR-2 is slightly emphasized by compression (Table 5). Most of the T-O-T angles of the 6-membered rings co-rotate and decrease with pressure. Table 5 also reports the features of the 4-membered rings present in wairakite framework (4mR-1, 4mR-2, 4mR-3, 4mR-4). At P_{amb}, the rings 4mR-1 (Fig. 4) and 4mR-3 (Fig. 6) are rather deformed and become more regular with increasing pressure (Table 5). On the contrary, 4mR-2 (Fig. 6) and 4mR-4 (Fig. 5) are square-shaped at P_{amb} and become more rhombic at 2.1 GPa (Table 5). These deformations are partially recovered upon pressure release. The opposite compression behavior of the two couples of 4mR units can be explained by the connection of these rings in the singly connected 4-ring chains of wairakite framework, which impose deformations along opposite directions (Gottardi and Galli 1985). The opposite deformation of the 6-membered rings along [111] can be similarly explained.

In wairakite framework, tetragonal prisms formed by two 4-rings and two 8-rings develop along **a**, **b**, and **c**. In particular, the prisms elongated along **c** have the bases formed by 4 Si atoms (4mR-4), while two Al atoms are disposed at middle height of the 8-rings. All these prismatic cages are occupied by Ca atoms (Fig. 4). The prisms elongated along **b** have two Al atoms in the two independent 4-rings (4mR-2 and 4mR-3) forming their bases, and are alternatively occupied by Na atoms (Fig. 5). The prismatic cages elongated along **a** have two Al atoms in the 4-rings (4mR-1) and are not occupied by extra-framework cations (Fig. 6). As visible in Figures 4–6, these prismatic units are strongly deformed upon compression, both in the 4-rings and in the 8-rings.

The results of the structural analysis reported in Tables 3–5 indicate that the *P*-induced framework deformations are only partially recovered upon decompression, in spite of the substantial reversibility of the unit-cell parameters.

Extra-framework species. At ambient pressure the Ca cations (M2 site) are coordinated by a pair of water molecules (WA,

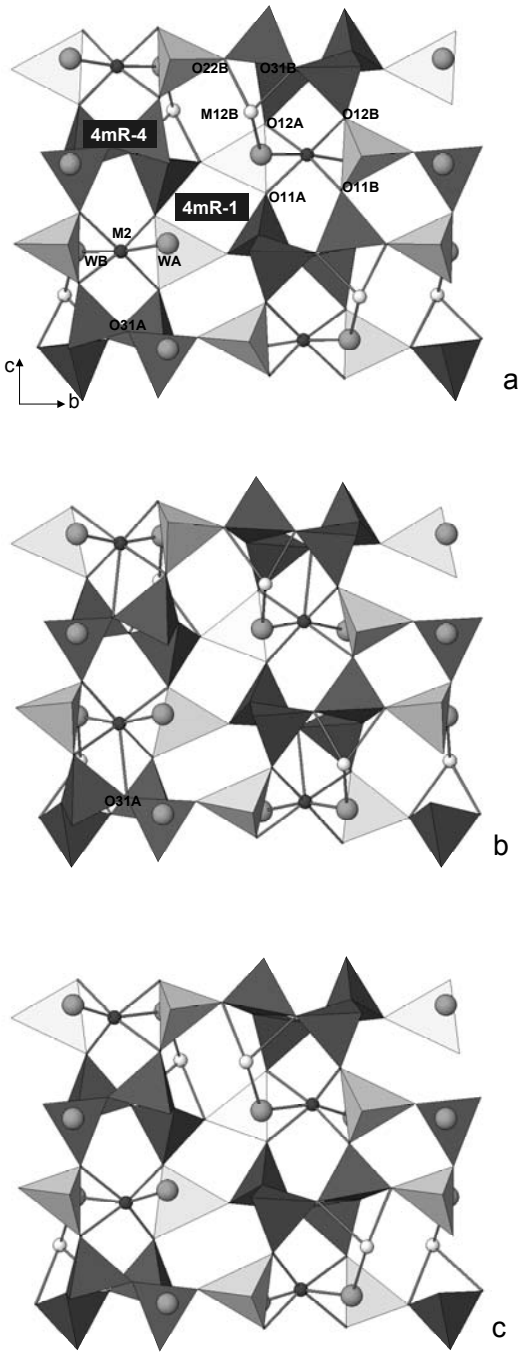

FIGURE 4. Projection along [100] direction of wairakite structure at (**a**) P_{amb}, (**b**) 2.1 GPa, and (**c**) P_{amb}(rev). Only a thin section of the structure along the **a** axis is shown to allow a better vision of the *P*-induced framework deformations and of the extra-framework cation polyhedra. Symbols 4mR-1 and 4mR-4 refer to two of the four 4-membered rings present in the wairakite framework (see also Table 5). At P_{amb}, the rings 4mR-1 are rather deformed and become more square-shaped with increasing pressure. Calcium—always present in all the prismatic units elongated along **c**—contributes to sustain the structure along **b** direction, thanks to the preferential orientation of the Ca-O bonds forming its coordination polyhedron.

TABLE 3. Refined atomic positions and displacement parameters (Å²) of monoclinic wairakite at selected pressures

	P_{amb}				0.9 GPa				2.1 GPa	
	x/a	y/b	z/c	U_{iso}	x/a	y/b	z/c	U_{iso}	x/a	y/b
T11A	0.1107(8)	0.1580(9)	0.4186(8)	0.020(1)	0.1050(8)	0.1555(9)	0.4175(8)	0.020(1)	0.107(1)	0.151(1)
T11B	0.8711(9)	0.3369(9)	0.4020(8)	0.020(1)	0.8683(9)	0.3404(9)	0.402(1)	0.020(1)	0.868(1)	0.339(1)
T12A	0.4231(8)	0.131(1)	0.1597(9)	0.020(1)	0.4285(9)	0.136(1)	0.1575(9)	0.020(1)	0.429(1)	0.130(1)
T12B	0.5984(8)	0.3721(9)	0.1688(8)	0.020(1)	0.6012(8)	0.374(1)	0.1698(9)	0.020(1)	0.595(1)	0.383(1)
T2A	0.1746(8)	0.4064(8)	0.1364(9)	0.020(1)	0.1790(9)	0.409(1)	0.1388(9)	0.020(1)	0.190(1)	0.407(1)
T2B	0.851(1)	0.0861(9)	0.1201(9)	0.020(1)	0.852(1)	0.085(1)	0.1207(9)	0.020(1)	0.859(1)	0.082(1)
O11A	0.100(1)	0.355(2)	0.2249(9)	0.020(1)	0.102(1)	0.358(2)	0.227(1)	0.022(2)	0.112(2)	0.353(2)
O11B	0.902(2)	0.153(1)	0.2153(8)	0.020(1)	0.912(2)	0.151(2)	0.2138(9)	0.022(2)	0.931(2)	0.119(2)
O12A	0.388(1)	0.142(2)	0.4638(9)	0.020(1)	0.387(1)	0.128(2)	0.4659(9)	0.022(2)	0.356(3)	0.125(2)
O12B	0.604(1)	0.357(2)	0.4835(9)	0.020(1)	0.603(2)	0.352(2)	0.481(1)	0.022(2)	0.606(2)	0.339(2)
O21A	0.201(1)	0.113(2)	0.358(1)	0.020(1)	0.196(1)	0.115(2)	0.354(1)	0.022(2)	0.189(1)	0.121(2)
O21B	0.775(1)	0.401(2)	0.378(2)	0.020(1)	0.775(1)	0.409(2)	0.376(2)	0.022(2)	0.761(1)	0.390(2)
O22A	0.134(2)	0.461(1)	0.389(2)	0.020(1)	0.127(2)	0.460(1)	0.387(2)	0.022(2)	0.136(2)	0.455(1)
O22B	0.838(1)	0.0323(9)	0.358(2)	0.020(1)	0.824(1)	0.035(1)	0.344(2)	0.022(2)	0.821(1)	0.033(1)
O31A	0.390(2)	0.2249(9)	0.096(2)	0.020(1)	0.403(2)	0.2261(9)	0.084(1)	0.022(2)	0.414(2)	0.231(1)
O31B	0.648(1)	0.278(1)	0.118(1)	0.020(1)	0.645(2)	0.275(1)	0.123(2)	0.022(2)	0.638(2)	0.275(1)
O32A	0.4864(9)	0.385(2)	0.134(2)	0.020(1)	0.494(1)	0.397(1)	0.122(2)	0.022(2)	0.496(1)	0.409(2)
O32B	0.5406(8)	0.125(2)	0.165(1)	0.020(1)	0.5449(9)	0.114(2)	0.164(2)	0.022(2)	0.546(1)	0.101(2)
M2*	0.0157(7)	0.245(1)	0.120(1)	0.049(3)	0.0160(7)	0.242(1)	0.1180(9)	0.041(3)	–. 003(2)	0.251(3)
M12B†	0.75	0.396(6)	0.00	*0.040*	0.75	0.377(7)	0.00	*0.040*	0.75	0.36(2)
WA	0.141(2)	0.119(2)	0.142(2)	0.057(5)	0.144(2)	0.124(2)	0.141(2)	0.038(6)	0.146(4)	0.134(5)
WB	0.899(2)	0.368(2)	0.118(2)	0.057(5)	0.906(2)	0.379(2)	0.123(2)	0.038(6)	0.891(4)	0.365(5)

Note: Values in italics correspond to structural parameters not refined during the fit procedure.
* Occupancy factor for M2 is 0.91, 0.92, 0.92, 0.94 for GPa P_{amb}, 0.9, 2.1 GPa, P_{amb}(rev), respectively.
† Occupancy factor for M12B is 0.28 GPa for all the refinements.

TABLE 4. T-O framework distances and coordination distances (<3.15 Å) of the extra-framework species for selected refinements of monoclinic wairakite

	P_{amb}	0.9 GPa	2.1 GPa	P_{amb}(rev)		P_{amb}	0.9 GPa	2.1 GPa	P_{amb}(rev)
T11A-O12A	1.611(2)	1.611(2)	1.622(7)	1.611(2)	T12B-O11B	1.611(2)	1.612(2)	1.621(7)	1.610(2)
T11A-O21A	1.610(2)	1.610(2)	1.628(7)	1.611(2)	T12B-O22B	1.610(2)	1.610(2)	1.632(7)	1.610(2)
T11A-O31A	1.611(2)	1.611(2)	1.624(7)	1.611(2)	T12B-O31B	1.610(2)	1.610(2)	1.619(7)	1.611(2)
T11A-O32A	1.610(2)	1.610(2)	1.620(7)	1.610(2)	T12B-O32A	1.611(2)	1.610(2)	1.617(7)	1.610(2)
mean	1.610	1.610	1.623	1.620	mean	1.610	1.610	1.622	1.620
T11B-O12B	1.611(2)	1.611(2)	1.622(7)	1.611(2)	T2A-O11A	1.730(2)	1.730(2)	1.716(8)	1.731(2)
T11B-O21B	1.610(2)	1.610(2)	1.618(7)	1.610(2)	T2A-O12A	1.731(2)	1.730(2)	1.702(7)	1.730(2)
T11B-O31B	1.610(2)	1.610(2)	1.623(7)	1.610(2)	T2A-O21A	1.730(2)	1.730(2)	1.708(7)	1.731(2)
T11B-O32B	1.610(2)	1.610(2)	1.630(7)	1.611(2)	T2A-O22B	1.730(2)	1.730(2)	1.711(8)	1.730(2)
mean	1.610	1.610	1.623	1.620	mean	1.730	1.730	1.709	1.730
T12A-O11A	1.611(2)	1.611(2)	1.631(7)	1.611(2)	T2B-O11B	1.730(2)	1.731(2)	1.711(8)	1.730(2)
T12A-O22A	1.610(2)	1.610(2)	1.630(7)	1.611(2)	T2B-O12B	1.730(2)	1.730(2)	1.715(7)	1.731(2)
T12A-O31A	1.611(2)	1.611(2)	1.624(7)	1.610(2)	T2B-O21B	1.730(2)	1.730(2)	1.704(8)	1.730(2)
T12A-O32B	1.611(2)	1.610(2)	1.628(7)	1.611(2)	T2B-O22A	1.730(2)	1.730(2)	1.717(7)	1.731(2)
mean	1.611	1.610	1.628	1.620	mean	1.730	1.730	1.712	1.730
M2-O11A	2.36(2)	2.44(3)	2.56(4)	2.45(6)	M12B-O22B	2.48(4)	2.62(5)	2.7(1)	2.70(9)
M2-O11B	2.38(2)	2.28(2)	2.39(4)	2.59(6)	M12B-O22B	2.48(4)	2.62(5)	2.7(1)	2.70(9)
M2-O12A	2.33(3)	2.48(3)	2.82(4)	2.53(6)	M12B-O31B	2.68(5)	2.59(6)	2.7(1)	2.9(1)
M2-O12B	2.56(2)	2.44(2)	2.23(3)	2.33(5)	M12B-O31B	2.68(5)	2.59(6)	2.7(1)	2.9(1)
M2-O31A		2.94(2)	2.97(4)		M12B-WB	2.62(3)	2.67(2)	2.51(5)	2.69(8)
M2-WA	2.45(3)	2.38(3)	2.58(7)	2.40(6)	M12B-WB	2.62(3)	2.67(2)	2.51(5)	2.69(8)
M2-WB	2.32(2)	2.38(2)	2.11(7)	2.46(5)					
WA-O11B			3.06(6)		WB-O11A	3.10(4)	3.00(3)		2.98(8)
WA-O21A	3.03(3)	2.93(3)	2.60(6)	2.94(7)	WB-O12A	3.13(3)	3.06(3)		
WA-O21B		3.14(3)			WB-O32B	3.04(4)	2.93(3)	2.86(7)	2.89(9)

WB) and by four framework O atoms belonging to a pair of Al tetrahedra, forming a rather regular octahedron (Fig. 4, Table 4). The small amount of Na is located in M12B site, octahedrally coordinated by four framework O atoms and by two WB water molecules, with bond distances larger than those of M2 octahedron (Figs. 5 and 6, Table 4). In this way, a cluster of two Ca and one Na polyhedra, bridged by WB water molecules, are formed (Figs. 4–6). At 0.9 and 2.1 GPa, a further framework O atom (O31A) approaches Ca cation at a rather long distance (2.94 and 2.97 Å, respectively), increasing Ca coordination number from six to seven (Table 4). On the contrary, no significant variations are observed in the Na polyhedra and in the extra-framework polyhedral connections.

Concerning the variation of the water molecule environment with pressure, Table 4 shows a decrease of WA-O21A and WB-O32B bond lengths and the appearance/disappearance of some weak water-framework interactions. The water-cation bonds generally strengthen upon compression.

TABLE 3.—*Continued*

2.1 GPa		P_{amb}(rev)			
z/c	U_{iso}	x/a	y/b	z/c	U_{iso}
0.411(1)	0.041(7)	0.110(2)	0.166(2)	0.411(2)	0.029(2)
0.392(1)	0.041(7)	0.872(2)	0.336(2)	0.401(2)	0.029(2)
0.161(2)	0.041(7)	0.420(2)	0.130(3)	0.165(2)	0.029(2)
0.175(1)	0.041(7)	0.593(2)	0.375(2)	0.165(2)	0.029(2)
0.141(1)	0.041(7)	0.172(2)	0.401(2)	0.131(3)	0.029(2)
0.106(1)	0.041(7)	0.846(3)	0.083(2)	0.110(2)	0.029(2)
0.225(2)	0.024(8)	0.092(4)	0.357(5)	0.218(2)	0.022(3)
0.206(1)	0.024(8)	0.883(5)	0.135(4)	0.219(2)	0.022(3)
0.475(1)	0.024(8)	0.387(4)	0.143(5)	0.472(2)	0.022(3)
0.488(1)	0.024(8)	0.612(5)	0.340(4)	0.482(2)	0.022(3)
0.328(2)	0.024(8)	0.203(2)	0.115(6)	0.359(4)	0.022(3)
0.367(3)	0.024(8)	0.777(3)	0.398(5)	0.368(5)	0.022(3)
0.396(2)	0.024(8)	0.141(4)	0.457(2)	0.386(4)	0.022(3)
0.345(2)	0.024(8)	0.847(5)	0.023(3)	0.341(4)	0.022(3)
0.095(2)	0.024(8)	0.380(4)	0.217(2)	0.096(4)	0.022(3)
0.144(2)	0.024(8)	0.644(4)	0.279(2)	0.121(4)	0.022(3)
0.109(2)	0.024(8)	0.483(2)	0.395(4)	0.126(5)	0.022(3)
0.169(2)	0.024(8)	0.538(2)	0.131(5)	0.167(4)	0.022(3)
0.108(2)	0.022(9)	0.007(2)	0.235(2)	0.117(2)	0.047(7)
0.00	*0.040*	0.75	0.41(1)	0.00	*0.040*
0.136(4)	*0.027*	0.139(4)	0.124(5)	0.152(4)	*0.057*
0.126(5)	*0.027*	0.891(5)	0.371(5)	0.133(5)	*0.057*

Note: Values in italics correspond to structural parameters not refined during the fit procedure.
* Occupancy factor for M2 is 0.91, 0.92, 0.92, 0.94 GPa for P_{amb}, 0.9, 2.1 GPa, P_{amb}(rev), respectively.
† Occupancy factor for M12B is 0.28 GPa for all the refinements.

TABLE 5. Structural features of the 4- and 6-tetrahedral rings present in the monoclinic wairakite structure at selected pressures

	P_{amb}	0.9 GPa	2.1 GPa	P_{amb}(rev)
6mR-1 [T2B-T11B-T12A-T2B-T11B-T12A]				
O12B-O12B (Å)	4.86(5)	4.93(5)	5.22(6)	5.36(15)
O22A-O22A (Å)	4.89(5)	4.74(5)	4.76(6)	5.10(13)
O32B-O32B (Å)	5.73(5)	5.50(5)	5.38(7)	5.86(12)
ε*	0.85	0.88	0.93	0.89
T11B-O32B-T12A (°)	135.3(14)	128.7(14)	122.8(13)	139.0(40)
T12A-O22A-T2B (°)	142.8(17)	147.7(17)	136.8(16)	144.0(40)
T2B-O12B-T11B (°)	141.6(14)	136.9(13)	130.6(17)	133.4(31)
6mR-2 [T2A-T11A-T12A-T2A-T11A-T12A]				
O11A-O11A (Å)	5.05(4)	5.01(5)	4.68(6)	5.29(14)
O31A-O31A (Å)	5.74(4)	6.17(4)	6.11(6)	5.61(12)
O21A-O21A (Å)	4.95(5)	4.83(6)	4.40(5)	4.91(15)
ε†	0.87	0.80	0.74	0.91
T2A-O21A-T11A (°)	142.6(15)	142.6(15)	123.1(19)	143.0(40)
T11A-O31A-T12A (°)	149.2(16)	141.3(14)	150.3(16)	138.0(40)
T12A-O11A-T2A (°)	138.5(14)	143.5(16)	139.8(16)	134.9(34)
4mR-1 [T2A-T12A-T2B-T12B]				
O22A-O22B (Å)	3.52(3)	3.35(3)	3.42(5)	3.22(8)
O11A-O11B (Å)	4.15(3)	4.06(4)	3.76(5)	3.92(9)
ε‡	0.85	0.82	0.91	0.82
T2A-O11A-T12A (°)	138.5(14)	143.5(16)	139.8(16)	134.9(34)
T12A-O22A-T2B (°)	142.8(17)	147.7(17)	136.8(16)	144.0(40)
T2B-O11B-T12B (°)	127.5(11)	122.0(12)	128.5(15)	149.0(40)
T12B-O22B-T2A (°)	150.6(15)	142.2(16)	141.0(15)	157.0(50)
4mR-2 [T2A-T11A-T2A-T11A]				
O21A-O21A (Å)	4.07(4)	4.17(4)	4.81(5)	4.04(10)
O12A-O12A (Å)	3.92(4)	3.85(4)	2.93(7)	3.83(11)
ε§	0.96	0.92	0.61	0.95
T11A-O12A-T2A (°)	146.1(15)	151.8(15)	175.6(18)	151.0(40)
T2A-O21A-T11A (°)	142.6(15)	142.6(15)	123.1(19)	143.0(40)
4mR-3 [T2B-T11B-T2B-T11B]				
O21B-O21B (Å)	3.39(5)	3.40(5)	3.54(7)	3.69(12)
O12B-O12B (Å)	4.02(4)	4.02(4)	3.89(6)	3.81(14)
ε‖	0.84	0.80	0.91	0.97
T11B-O21B-T2B (°)	149.9(17)	143.9(16)	152.9(19)	144.0(40)
T2B-O12B-T11B (°)	141.6(14)	136.9(13)	130.6(17)	133.4(31)
4mR-4 [T11A-T12A-T11B-T12B]				
O31A-O31B (Å)	3.61(3)	3.39(3)	3.12(4)	3.71(9)
O32A-O32B (Å)	3.65(3)	3.94(3)	4.29(3)	3.74(9)
ε#	0.99	0.86	0.73	0.99
T11A-O31A-T12A (°)	149.2(16)	141.3(14)	150.3(16)	138.0(40)
T12A-O32B-T11B (°)	135.3(14)	128.7(14)	122.8(13)	139.0(40)
T11B-O31B-T12B (°)	141.4(14)	148.7(16)	156.5(18)	144.0(40)
T12B-O32A-T11A (°)	150.6(15)	142.6(13)	132.0(12)	138.7(34)

* ε = 0.5[(O12B-O12B) + (O22A-O22A)]/[(O32B-O32B)].
† ε = 0.5[(O11A-O11A) + (O21A-O21A)]/[(O31A-O31A)].
‡ ε = [(O22A-O22B)/(O11A-O11B)].
§ ε = [(O12A-O12A)/(O21A-O21A)].
‖ ε = [(O21B-O21B)/(O12B-O12B)].
ε = [(O31A-O31B)/(O32A-O32B)].

Structural interpretation of the lattice parameters evolution

Due to the pseudo-cubic topological symmetry of wairakite, one could expect an isotropic compressional behavior; hence, the anisotropic evolution of the lattice parameters upon compression (Fig. 2) has been interpreted on the basis of the distribution of the extra-framework species and of the modifications of their coordination polyhedra. In particular, we focused our attention on the different distribution of the extra-framework cations inside the tetragonal prismatic cages previously described. Calcium—always present in all the prisms elongated along **c** axis—contributes to sustain the structure along **b** direction (Fig. 4), which is the less compressible parameter of wairakite cell. In fact, **b** contraction could induce an unacceptable shortening of the Ca-O_{frame} coordination bonds. On the contrary, the lacking of cations in the prisms developed along **a** direction, allows a larger deformation of the structure along **c**, the most compressible unit-cell axis (Fig. 6). The contraction of **a** unit-cell axis up to about 5 GPa and its stabilization above this pressure, can be interpreted as due to the presence of sodium atoms in one half of the tetragonal prisms developed along **b** (Fig. 5) with an occupancy of 0.28 (Table 3). This partial occupancy of the Na sites could prevent the further contraction along **a** in the last stages of compression.

DISCUSSION

Comparing the compressibility and the *P*-induced structural deformations of the related zeolites analcime (Gatta et al. 2006) and wairakite, we observe some similarities and some differences. In particular, in both phases no complete amorphization is observed up to 7.0 and 7.8 GPa for analcime and wairakite, respectively; moreover the original unit-cell parameters are substantially recovered upon decompression to P_{amb}. In both the ANA zeolites, a transition to a triclinic phase is observed, with an increase of compressibility after the transition pressure. A similar behavior of the HP polymorph has been already observed for zeolite scolecite (Ballone et al. 2002), sheet silicates (Welch et al. 2004), carbonates (Singh and Kennedy 1974; Martinez et al. 1996; Smyth and Ahrens 1997; Redfern 2000; Holl et al. 2000), and gillespite-type phases (Miletich 2000). The bulk modulus of triclinic analcime [19(2) GPa] and triclinic wairakite [24(3) GPa] are similar to each other and are among the lowest up to now found for zeolites; in particular, the bulk modulus of triclinic analcime is higher only than that of Li-RHO phase (17

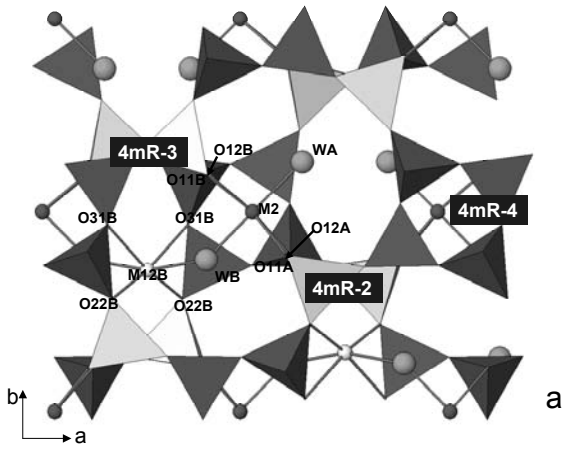

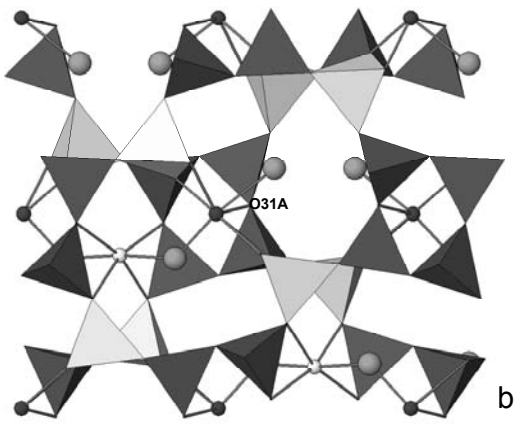

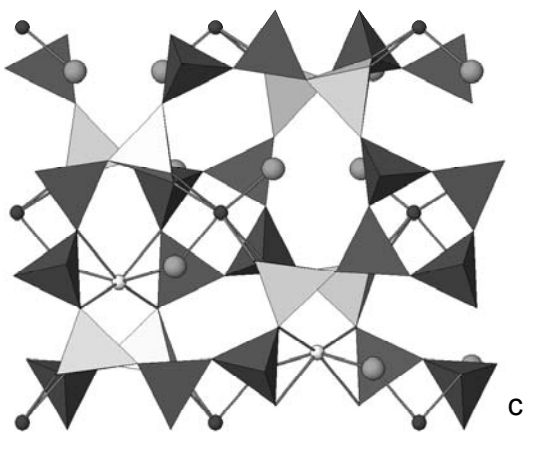

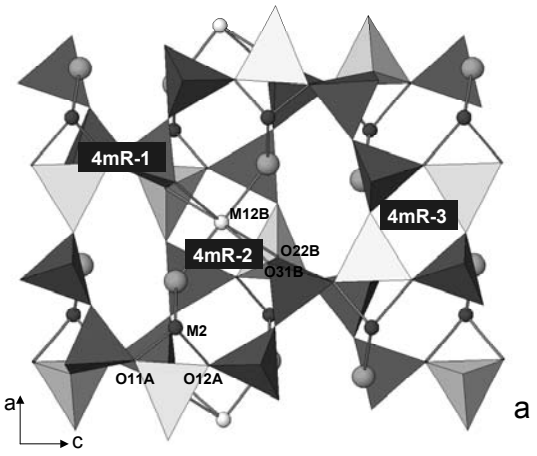

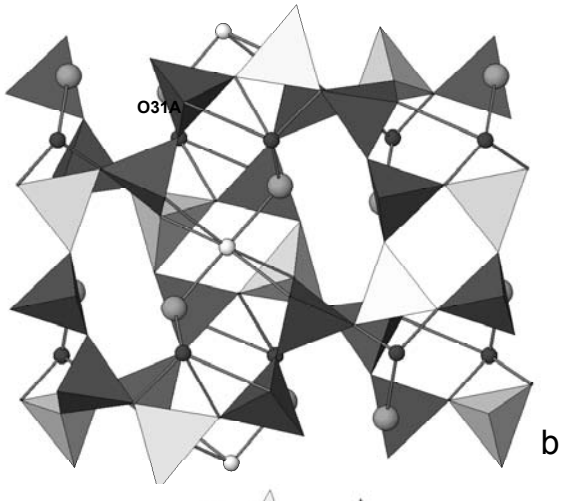

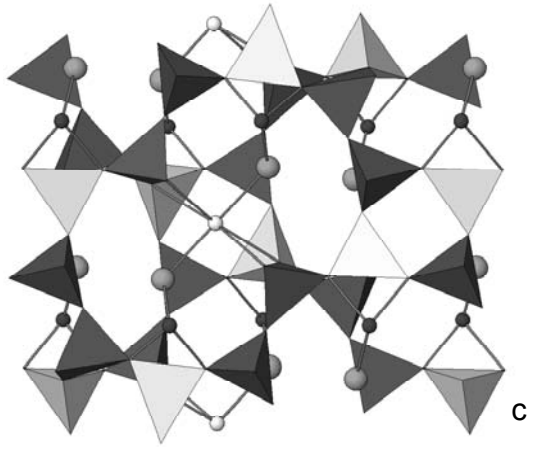

FIGURE 5. Projection along [001] direction of wairakite structure at (**a**) P_{amb}, (**b**) 2.1 GPa, and (**c**) P_{amb}(rev). Only a thin section of the structure along **c** axis is shown to allow a better vision of the *P*-induced framework deformations and of the extra-framework cation polyhedra. Symbols 4mR-2, 4mR-3, and 4mR-4 refer to three of the four 4-membered rings present in the wairakite framework (see also Table 5). 4mR-4 rings are square-shaped at P_{amb} and become rhombic at 2.1 GPa. These deformations are partially recovered upon pressure release. The prismatic units developed along **b** are strongly deformed upon compression, both in the 4- and in the 8-rings, and becomes pear-like shaped.

FIGURE 6. Projection along [010] direction of wairakite structure at (**a**) P_{amb}, (**b**) 2.1 GPa, and (**c**) P_{amb}(rev). Only a thin section of the structure along **b** axis is shown to allow a better vision of the *P*-induced framework deformations and of the extra-framework cation polyhedra. Symbols 4mR-1, 4mR-2, and 4mR-3 refer to three of the four 4-membered rings present in the wairakite framework (see also Table 5). These 4mR-2 rings are square-shaped at P_{amb} and become rhombic at 2.1 GPa. These deformations are partially recovered upon pressure release. The prismatic units developed along **a** are strongly deformed upon compression, both in the 4- and in the 8-rings, due to the absence of extra-framework cations inside.

GPa) (Lee et al. 2001).

On the basis of the structural refinements of monoclinic wairakite, we see that the framework deformation mechanism is basically driven by tetrahedral tilting-as for all the other zeolites studied under high pressure-and in particular it is similar to that of analcime as concerns the deformation of the 4mR-, 6mR-, and 8mR-rings. Finally, in both the ANA zeolites, the *P*-induced deformation brings more oxygen framework atoms in the coordination polyhedra of the extra-framework cations, increasing their coordination number from 6 to 7.

Some significant differences can be singled out in the HP behavior of the two phases. Wairakite transition from monoclinic to triclinic phase occurs above 2.5 GPa, while the transition from cubic to triclinic analcime occurs at about 1 GPa. This effect, and the lower compressibility of cubic analcime [K_0 = 56(3), Gatta et al. 2006] with respect to that of monoclinic wairakite [K_0 = 39(3), this work], can be reasonably attributed to the higher capacity of monoclinic structure to accommodate the HP-induced strains with respect to the more constrained cubic one. This interpretation is strengthened by the evidence that, when both frameworks become triclinic, the bulk moduli are similar to each other [19(2) and 24(3) for analcime (Gatta et al. 2006) and wairakite, respectively]. Moreover, the HP-response of the triclinic analcime unit-cell parameters is more isotropic than that of triclinic wairakite. This can be attributed to the different chemical nature and distribution of the extra-framework cations in the two zeolites. In analcime, in fact, Na cations statistically occupy all the tetragonal prisms, while in wairakite different cationic species (Ca and Na) occupy some of these units, and others are empty.

It is now interesting to compare the deformation behavior of wairakite under HP and HT conditions. In the first stages of heating (Seryotkin et al. 2003), wairakite undergoes a unit-cell volume increase of about 2%; then, after a phase transition from monoclinic to tetragonal symmetry, the dehydration process starts and the cell volume decreases down to a value very similar to the original one. Hence, as a whole, wairakite is very rigid upon heating while, on the contrary, is much more flexible upon compression. We can thus assert that wairakite shares with analcime (Cruciani and Gualtieri 1999; Gatta et al. 2006), bikitaite (Ferro et al. 2002, 2004; Comodi et al. 2003), mordenite (Martucci et al. 2003; Gatta and Lee 2006), and zeolite A (Pluth and Smith 1980; Arletti et al. 2003), a strong rigidity under HT and a high deformability under HP. An opposite behavior is otherwise observed for the fibrous zeolites natrolite, scolecite, edingtonite (Gatta et al. 2004a, 2004b; Gatta 2005), heulandite (Alberti and Vezzalini 1983; Comodi et al. 2001; Vezzalini et al. 2001), yugawaralite (Alberti et al. 1996; Artioli et al. 2001; Fois et al. 2005a, 2005b), and gismondine (Vezzalini et al. 1993; Betti et al. 2007), which are flexible under both HP and HT conditions, though to a different extent.

Acknowledgments

This work was supported by the Italian MIUR (PRIN2004 "Stabilita' delle zeoliti in condizioni chimico-fisiche non ambientali: dalle modificazioni strutturali alle modellizzazioni atomistiche"). The Swiss-Norwegian beamline (BM01) at European Synchrotron Radiation Facility is acknowledged for allocation of beamtime under proposal no. 01-02-723 and for technical support during the experiments. Comments of M. Kunz (Associate Editor), G. Diego Gatta, and an anonymous reviewer helped improve the manuscript .

References cited

Alberti, A. and Vezzalini, G. (1983) The thermal behavior of heulandites: A structural study of the dehydration of Nadap heulandite. Tschermaks Mineralogische und Petrographische Mitteilungen, 31, 259–270.

Alberti, A., Quartieri, S., and Vezzalini, G. (1996) Thermal behavior of zeolites: Single crystal X-ray study of dehydration and rehydration mechanism in yugawaralite. European Journal of Mineralogy, 8, 1273–1282.

Angel, R.J. (2001) EOS-FIT V5.2. Computer program. Crystallography Laboratory, Deparment of Geological Sciences, Virginia Tech, Blacksburg, U.S.A.

Arletti, R., Ferro, O., Quartieri, S., Sani, A., Tabacchi, G., and Vezzalini, G. (2003) Structural deformation mechanisms of zeolites under pressure. American Mineralogist, 88, 1416–1422.

Artioli, G., Ståhl, K., Cruciani, G., Gualtieri, A., and Hanson, J.C. (2001) In situ dehydration of yugawaralite. American Mineralogist, 86, 185–192.

Baerlocher, C., Meier, W.M., and Olson, D.H. (2001) Atlas of zeolite framework types. Elsevier, Amsterdam.

Ballone, P., Quartieri, S., Sani, A., and Vezzalini, G. (2002) High-pressure deformation mechanism in scolecite: a combined computational-experimental study. American Mineralogist, 87, 1194–1206.

Betti, C., Fois, E., Mazzuccato, E., Medici, C., Quartieri, S., Tabacchi, G., Vezzalini, G., and Dmitriev, V. (2007) Gismondine under HP: Deformation mechanism and re-organization of the extra-framework species. Microporous and Mesoporous Materials, 103, 190–209.

Birch, F. (1947) Finite elastic strain of cubic crystal. Physical Review, 71, 809–824.

Bish, D.L. and Ming, D.W., Eds. (2001) Natural zeolites: Occurrence, properties, applications, vol. 45. Reviews in Mineralogy and Geochemistry, Mineralogical Society of America, Chantilly, Virginia.

Comodi, P., Gatta, G.D., and Zanazzi, P.F. (2001) High-pressure structural behaviour of heulandite. European Journal of Mineralogy, 13, 497–505.

——— (2003) Effects of pressure on the structure of bikitaite. European Journal of Mineralogy, 15, 267–295.

Coombs, D.S., Alberti, A., Armbruster, T., Artioli, G., Colella, C., Galli, E., Grice, J.D., Liebau, F., Mandarino, J.A., Minato, H., Nickel, E.H., Passaglia, E., Peacor, D.R., Quartieri, S., Rinaldi, R., Ross, M., Sheppard, R.A., Tillmanns, E., and Vezzalini, G. (1997) Recommended nomenclature for zeolite minerals: Report of the Subcommittee on Zeolites of International Mineralogical Association, Commission on New Minerals and Minerals Names. Canadian Mineralogist, 35, 1571–1606.

Cromer, D.T. and Waber, J.R. (1974) Atomic scattering factors for X-rays. In J.A. Ibers and W.C. Hamilton, International Tables for X-ray Crystallography, Vol. IV, Section 2.2, p. 99–101. The Kynoch Press, Birmingham, U.K.

Cruciani, G. and Gualtieri, A. (1999) Dehydration dynamics of analcime by in situ synchrotron powder diffraction. American Mineralogist, 84, 112–119.

Donovan, J.J. (1995) PROBE: PC-based data acquisition and processing for electron microprobes. Advanced Microbeam, Vienna, Ohio.

Fei, Y. and Wang, Y. (2000) High-pressure and high-temperature powder diffraction. In R.M. Hazen and R.T. Downs, Eds., High-temperature and High-pressure Crystal Chemistry, 41, 521–557. Reviews in Mineralogy and Geochemistry, Mineralogical Society of America, Chantilly, Virginia.

Ferro, O., Quartieri, S., Vezzalini, G., Fois, E., Gamba, A., and Tabacchi, G. (2002) High-pressure behavior of bikitaite: an integrated theoretical and experimental approach. American Mineralogist, 87, 1415–1425.

Ferro, O., Quartieri, S., Vezzalini, G., Ceriani, C., Fois, E., Gamba, A., and Cruciani, G. (2004) Dehydration dynamics of bikitaite: Part I. In situ synchrotron powder X-ray diffraction study. American Mineralogist, 89, 94–101.

Fois, E., Gamba, A., Tabacchi, G., Arletti, R., Quartieri, S., and Vezzalini, G. (2005a) The "template" effect of the extra-framework content on zeolite compression: the case of yugawaralite at high pressure. American Mineralogist, 90, 28–35.

——— (2005b) High-pressure behaviour of yugawaralite at different water content: an ab initio study. In A. Gamba, C. Colella, and S. Coluccia, Eds., Oxide based materials, studies in surface science and catalysis series, 155, p. 271. Elsevier Science B.V., Amsterdam.

Forman, R.A., Piermarini, G.J., Barnett, J.D., and Block, S. (1972) Pressure measurements made by utilization of the ruby sharp-line luminescence. Science, 176, 284–286.

Gatta, G.D. (2005) A comparative study of fibrous zeolites under pressure. European Journal of Mineralogy, 17, 411–421.

Gatta, G.D. and Lee, Y. (2006) On the elastic behavior of zeolite mordenite: A synchrotron powder diffraction study. Physics and Chemistry of Minerals, 32, 726–732.

Gatta, G.D., Boffa Ballaran, T., Comodi, P., and Zanazzi, P.F. (2004a) Isothermal equation of state and compressional behaviour of tetragonal edingtonite. American Mineralogy, 89, 633–639.

——— (2004b) Comparative compressibility and equation of state of orthorhombic and tetragonal edingtonite. Physics and Chemistry of Minerals, 31, 288–298.

Gatta, G.D., Nestola, F., and Boffa Ballaran, T. (2006) Elastic behavior, phase

transition, and pressure induced structural evolution of analcime. American Mineralogist, 91, 568–578.
Gottardi, G. and Galli, E. (1985) Natural Zeolites, 409 p. Springer-Verlag, Berlin.
Goryainov, S.V., Fursenko, B.A., and Belitsky, I.A. (1996) Phase transitions in analcime and wairakite at low-high temperatures and high pressure. Physics and Chemistry of Minerals, 23, 297–298.
——— (1999) Raman spectroscopy of phase transition and amorphyzation of wairakite at high pressure. Doklady Akademy Nauk, 369, 70–73.
Hammersley, A.P., Svensson, S.O., Hanfland, M., Fitch, A.N., and Häusermann, D. (1996) Two-dimensional detector software: from real detector to idealized image or two-theta scan. High Pressure Research, 14, 235–248.
Hazen, R.M. and Finger, L.W. (1979) Polyhedral tilting: a common type of pure displacive phase transition and its relationship to analcite at high pressure. Phase Transitions, 1, 1–22.
Henderson, C.M.B., Bell, A.M.T., Kohn, S.C., and Page, C.S. (1998) Leucite-pollucite structure-type variability and the structure of a synthetic end-member calcium wairakite ($CaAl_2Si_4O_{12}·2H_2O$). Mineralogical Magazine, 62, 165–178.
Holl, C.M., Smyth, J.R., Laustsen, H.M.S., Jacobsen, S.D., and Downs, R.T. (2000) Compression of witherite to 8 GPa and the crystal structure of $BaCO_3$-II. Physics and Chemistry of Minerals, 27, 467–473.
Larson, A.C. and Von Dreele, R.B. (1996) GSAS-General Structure Analysis System. Report LAUR 86-748, Los Alamos National Laboratory, Los Alamos, New Mexico.
Le Bail, A., Duroy, H., and Fourquet, J.L. (1988) Ab-initio structure determination of $LiSbWO_6$ by X-ray powder diffraction. Material Research Bulletin, 23, 447–452.
Lee, Y., Hriljac, J.A., Vogt, T., Parise, J.B., Edmondson, M.J., Anderson, P.A., Corbin, D.R., and Takaya, N. (2001) Phase transition of zeolite RHO at high-pressure. Journal of American Chemical Society, 123, 8418–8419.
Lee, Y., Vogt, T., Hriljac, J.A., Parise, J.B., and Artioli, G. (2002a) Pressure-induced volume expansion of zeolites in the natrolite family. Journal of American Chemical Society, 124, 5466–5475.
Lee, Y., Vogt, T., Hriljac, J.A., Parise, J.B., Hanson, J.C., and Kim, S.J. (2002b) Non framework cation migration and irreversible pressure-induced hydration in a zeolite. Nature, 420, 485–489.
Mao, H.K., Xu, J., and Bell, P.M. (1986) Calibration of the ruby pressure gauge to 800 kbar under quasi-hydrostatic conditions. Journal of Geophysical Research, 91, 4673–4676.
Martinez, I., Zhang, J., and Reeder, R.J. (1996) In situ X-ray diffraction of aragonite and dolomite at high pressure and high temperature: Evidence for dolomite breakdown to aragonite and magnesite. American Mineralogist, 81, 611–624.
Martucci, A., Sacerdoti, M., Cruciani, G., and Dalconi, C. (2003) In situ time resolved synchrotron powder diffraction study of mordenite. European Journal of Mineralogy, 15, 485–493.
Mazzi, F. and Galli, E. (1978) Is each analcime different? American Mineralogist, 63, 448–460.
Miletich, R. (2000) The tetragonal-to-tetragonal phase transition in gillespite-type phases. Is there elastic softening at high pressures? 8th International Symposium on Experimental Mineralogy, Petrology and Geochemistry (EMPG VIII), Bergamo, Italy, 16-19/4/2000, p. 71.
Miletich, R., Allan, D.R., and Kush, W.F. (2000) High-pressure single-crystal techniques. In R.M. Hazen and R.T. Downs, Eds., High-temperature and High-pressure Crystal Chemistry, 41, p. 445–519. Reviews in Mineralogy and Geochemistry, Mineralogical Society of America and Geochemical Society, Chantilly, Virginia.
Pluth, J.J. and Smith, J.V. (1980) Accurate redetermination of crystal structure of dehydrated zeolite A. Absence of near zero coordination of sodium. Refinement of silicon,aluminum-ordered superstructure. Journal of American Chemical Society, 102, 4704–4708.
Redfern, S.A.T. (2000) Structural variations in carbonates. In R.M. Hazen and R.T. Downs, Eds., High-temperature and High-pressure Crystal Chemistry, 41, p. 289–308. Reviews in Mineralogy and Geochemistry, Mineralogical Society of America, Chantilly, Virginia.
Seryotkin, Y.V., Joswig, W., Bakakin, V.V., Belitsky, I.A., and Fursenko, B.A. (2003) High-temperature crystal structure of wairakite. European Journal of Mineralogy, 15, 475–484.
Singh, A.K. and Kennedy, G.C. (1974) Compression of calcite to 40 kbar. Journal of Geophysical Research, 79, 2615–2622.
Smyth, J.R. and Ahrens, T.J. (1997) The crystal structure of calcite III. Geophysical Research Letters, 25, 1595–1598.
Steiner, A. (1955) Wairakite, the calcium analogue of analcime, a new zeolite mineral. Mineralogical Magazine, 30, 691–698.
Takeuchi, Y., Mazzi, F., Haga, N., and Galli, E. (1979) The crystal structure of wairakite. American Mineralogist, 64, 993–1001.
Thomson, P., Cox, D.E., and Hastings, J.B. (1987) Rietveld refinement of Debye-Scherrer synchrotron X-ray data from Al_2O_3. Journal of Applied Crystallography, 20, 79–83.
Toby, B.H. (2001) EXPGUI, a graphical user interface for GSAS. Journal of Applied Crystallography, 34, 210–213.
Tschernich, R.W. (1992) Zeolites of the word. Geoscience Press Inc., Phoenix, Arizona.
Vezzalini, G., Quartieri, S., and Alberti, A. (1993) Structural modifications induced by dehydration in the zeolite gismondine. Zeolites, 13, 34–42.
Vezzalini, G., Quartieri, S., Sani, A., and Levy, D. (2001) The structural modifications induced by high pressure in scolecite and heulandite: In-situ synchrotron X-ray powder diffraction study. In A. Galarneau, F. Di Renzo, F. Fajula, and J. Vedrine, Eds., Studies in surface sciences and catalysis, 135. Elsevier Science B.V., Amsterdam.
Weidner, D.J., Huang, Y., Chen, G., Hando, J., and Vaughan, M.T. (1998) Rheology measurements at high pressure and temperature. In M.H. Manghnani and T. Yagy, Eds., Properties of Earth and Planetary Materials at High Pressure and Temperature, p. 473–480. American Geophysics Union, Washington, D.C.
Welch, M.D., Kleppe, A.K., and Jephcoat, A.P. (2004) Novel high-pressure behavior in chlorite: A synchrotron XRD study of clinochlore to 27 GPa. American Mineralogist, 89, 1337–1340.
Werner, P.E., Eriksson, L., and Westdhal, M. (1985) TREOR, a semi-exhaustive trial-and-error powder indexing program for all symmetries. Journal of Applied Crystallography, 18, 367–370.
Yamanaka, T., Nagay, T., and Tsuchiya, T. (1997) Mechanism of pressure-induced amorphization. Zeitschrift für Kristallographie, 212, 401–410.

Manuscript received January 8, 2007
Manuscript accepted August 20, 2007
Manuscript handled by Martin Kunz